TECHNICAL NOTES

Dual Fluorescent Labeling Method to Visualize Plasmid DNA Degradation

Charudharshini Srinivasan,[⊥,†] Shafiuddin Siddiqui,[#,‡] Lawrence K. Silbart,[§] Fotios Papadimitrakopoulos,[||] and Diane J. Burgess*[,†]

Department of Pharmaceutical Sciences, University of Connecticut, 69 North Eagleville Road, Unit 3092; Department of Animal Science, Center of Excellence for Vaccine Research, University of Connecticut, 1390 Storrs Road, Unit 4163; Department of Allied Health Sciences, Center of Excellence for Vaccine Research, University of Connecticut, 358 Mansfield Road; and Nanomaterials Optoelectronics Laboratory, Polymer Program, Department of Chemistry, Institute of Materials Science, University of Connecticut, 97 North Eagleville Road, Unit 3136, Storrs, Connecticut 06269. Received May 8, 2008; Revised Manuscript Received November 11, 2008

The efficiency of nonviral vectors for gene delivery may be enhanced by understanding the key barriers that limit the translocation of the therapeutic DNA into the nucleus. One such barrier is the instability of DNA in the cytoplasm. In this work, we have developed a method to dual-label plasmid DNA to be utilized as a tool to elucidate DNA instability during its trafficking in the intracellular microenvironment. Plasmid DNA containing rhodamine and maleimide groups linked using peptide nucleic acid (PNA) linkers was utilized for conjugation. Covalent conjugation of the maleimide group with a second fluorophore, fluorescein, did not alter the electrophoretic mobility or the structural integrity of the DNA, as confirmed by gel electrophoresis. The intact DNA was visualized as a single color (yellow) due to the close proximity of the green and red fluorophores. DNA degradation was simulated using restriction endonucleases (*Bam*H1 and *Pfl*MI) to cut the DNA at two or more sites resulting in color separation. Confocal time-lapse imaging was utilized to follow DNA stability upon incubation of Lipofectamine2000/dual-labeled DNA complexes in CHO-K1 cells. Yellow fluorescent voxels were seen in the cell cytoplasm indicating the presence of intact DNA. Red and green fluorescent voxels were also seen in a few cells, suggesting separation of the fluorophores and probable DNA degradation. The methodology developed in this report provides a new tracking tool for investigators to explore DNA degradation at the molecular level inside single cell.

INTRODUCTION

Transfection of therapeutic DNA mediated by nonviral gene delivery has been investigated over the past three decades as a safer alternative to viral vectors for use in the treatment of genetic, infectious, and acquired diseases (*1*−*6*). However, the transfection efficiencies that can be achieved using nonviral vectors are relatively low when compared to viral-based delivery systems (*4, 7, 8*). Although several different approaches have been investigated to enhance transfection, success has been limited and low efficiency remains a concern (*9*−*12*). Consequently, only approximately 26% of all gene therapeutics in clinical trials utilize nonviral vectors, whereas approximately 68% utilize viral vectors (the remaining 6% utilize RNA transfer, yeast, bacterial, or unknown vectors) (http://www.wiley.co.uk/genmed/clinical) (*13*).

Gene trafficking is being investigated to understand the barriers that hinder the translocation of nonviral vectors and their payload from outside the cell into the nucleus (*11, 14*−*19*). Such information could then be used to redesign nonviral vectors for improved transfection. Gene trafficking of nonviral vectors involves cellular binding and uptake, endosomal escape, safe transport through cytosol, and nuclear delivery. Several reviews have been recently published that describe gene trafficking in detail and the dependency of the trafficking process on the nature of the delivery vector (*5, 11, 20*−*22*). Depending on the vector used, one or more of these steps may limit transfection efficiency.

Cellular binding and uptake of gene delivery vectors is well-understood and depends on the interaction between the vector and the cell surface (*5, 7, 11, 12*). Vectors are usually transported into the cell in endosomes. The environment within the endosomes (low pH and the presence of nucleases) is hostile to DNA. Much research has been conducted and vectors have been developed that promote rapid escape from endosomes (such as fusogenic lipids, peptides, and lysosomotropic agents *23*−*25*). Depending on the nature of the vector, the DNA may be released

* To whom correspondence and reprint requests should be addressed. Department of Pharmaceutical Sciences, University of Connecticut, 69 North Eagleville Road, Unit 3092, Storrs, CT 06269, USA. Phone: 860-486-3760. Fax: 860-486-0538. E-mail: d.burgess@uconn.edu.

† Department of Pharmaceutical Sciences.

‡ Department of Animal Science, Center of Excellence for Vaccine Research.

§ Department of Allied Health Sciences, Center of Excellence for Vaccine Research.

|| Institute of Materials Science.

⊥ Current address: Immune Disease Institute, Harvard Medical School, 3 Black Fan Circle, 3rd Floor, Rm 3024, Boston, MA 02115. E-mail: csrinivasan@idi.harvard.edu.

Current address: 77 Avenue Louis Pasteur, Room 720, Harvard Institute of Medicine, Center for Neurological Disease, Boston, MA 02115. Email: ssiddiqui1@bics.bwh.harvard.edu.

10.1021/bc800184j CCC: $40.75
Published on Web 12/16/2008

into the cytoplasm together with the vector or as free DNA. Free DNA is subject to degradation by the many endo- and exonucleases that are present in the cell. Although the majority of these reside in the nucleus, some are located within the cytoplasm (*26, 27*). Degradation of free DNA by nucleases present in the cytoplasm may be considerable due to the significant time required for transport through the cytoskeletal network (*22*). Finally, the DNA must be translocated into the nucleus that may occur by passive entry during mitotic cell division and/or by active process through pores in the nuclear membrane. This is dependent on the DNA conformation as well as cellular characteristics (*28, 29*). Although much work has been conducted to understand these transport processes, the amount of DNA lost at these various steps is unknown. For example, although a vector may be designed to promote endosomal escape, some DNA may be degraded prior to escape. Consequently, it would be useful to have a method to track DNA degradation throughout the entire trafficking process.

To date, there are only a few reports that describe investigations into DNA degradation. These include studying nuclease activity on plasmid DNA with different cytosolic extracts using gel electrophoresis (*30, 31*); monitoring intracellular disappearance of DNA by fluorescence in situ hybridization (FISH); visualization of plasmid DNA fragmentation using terminal deoxynucleotidyl transferase-mediated dUTP nick end labeling (TUNEL) assay; and radiolabeled ^{32}P-release from end-labeled fragmented DNA (*30, 31*). These studies have provided important information on the effect of cytosolic nucleases on DNA, but are limited since they have been performed using microinjected materials in single cells and require isolated cell fractions or fixed cells, which may not represent events that occur in living cells (*30, 31*).

Investigations based on labeling techniques have involved monitoring gold-labeled DNA by transmission electron microscopy (TEM) (*32, 33*) and single dye labeled delivery vector/DNA (oligonucleotides or plasmid DNA) by confocal imaging (*34, 35*). TEM only provides static images of cells, and the dye labeled DNA complexes have been imaged immediately following microinjection and therefore lack critical information about DNA stability once released from the complex.

On the basis of the above, there is a great need to develop a tool to monitor real-time degradation processes in live cells. Live cell tracking is commonly performed using fluorescent dyes to label biomolecules such as antibodies, peptides (*36*), and small oligonucleotides (*37, 38*). Labeling of plasmid DNA can be challenging, since chemical modification may render the DNA nonfunctional (*39*−*41*). However, we have previously demonstrated successful labeling of plasmid DNA with quantum dots using peptide nucleic acid (PNA) chemistry without loss of functionality for long-term single cell tracking studies (*19*).

In this study, we have demonstrated a novel approach to monitor plasmid DNA degradation that utilizes dual-labeled DNA as a probe. The DNA was labeled with two different fluorophores (rhodamine and fluorescein) via PNA linkers. The two dyes are expected to be seen as a single color in intact DNA due to colocalization, but when the DNA strands are broken and the segments move apart, color separation may be observed. This concept was demonstrated using restriction enzymes to cut the DNA. Confocal time-lapse imaging was used to follow cellular uptake of DNA as well as probable degradation, as demonstrated by color separation, occurring within the cytoplasm. The plasmid DNA was shown to have retained its structural integrity following dual labeling. This dual-labeling technique provides a novel approach to visualize plasmid DNA instability at a single cell level throughout the trafficking pathway.

Scheme 1. Schematic Illustration of pGeneGrip-gWIZ DNA Dual-Labeled with Fluorescein and Rhodamine Labels at Site-1 and and Site-2, Respectively[a]

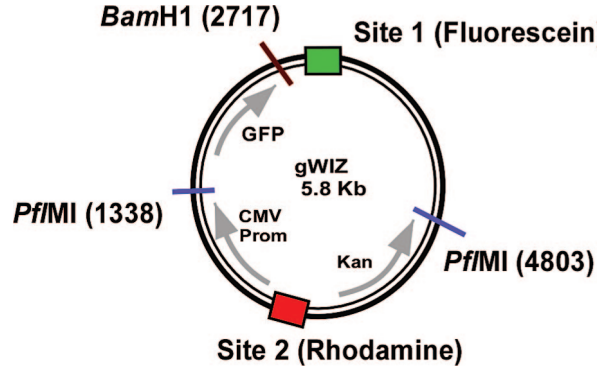

[a] The plasmid with restriction enzymes (*Bam*H1 and *Pfl*MI) used to digest at single and double recognition sites, respectively, on the dual-labeled plasmid DNA are shown.

MATERIALS AND METHODS

Plasmid DNA Preparation. Green fluorescent protein encoding pGeneGrip-gWIZ plasmid DNA (∼5.8 kb) with hCMV IE promoter−enhancer gene sequence was purchased from Genlantis (San Diego, CA). The pGeneGrip plasmid contains two PNA binding sites (sites −1 and −2) that are attached to maleimide and rhodamine (Rh) labels through PNA linkers, respectively (*19, 40*). The general method for chemical conjugation of plasmid DNA to PNA linkers has been reported in detail in our previously published work (*19*). The total concentration and purity of DNA in solution was determined spectroscopically at 260 and 280 nm using a Beckman DU 7400 spectrophotometer. Plasmid DNA structural integrity was analyzed using a 0.8% w/v DNA agarose gel.

Dual Labeling of Plasmid DNA with Fluorophores. pGeneGrip-gWIZ plasmid was dual-labeled by covalent conjugation of the maleimide group at site-1 with fluorescein (Schemes 1 and 2). For this reaction, 5-((2-(and-3)-*S*-(acetylmercapto)succinoyl)amino)fluorescein (SAMSA fluorescein, A-685) (**1**) (Molecular probes, Invitrogen Corp., Carlsbad, CA) was utilized as a fluorophore (Scheme 2). It was activated prior to the conjugation reaction to expose free thiol residues as described below (Scheme 2).

Activation of SAMSA Fluorescein. Activation of **1** was performed by incubating the stock solution (10 mg/mL) of SAMSA fluorescein prepared in 0.1 N sodium hydroxide for 15 min at room temperature. It was then neutralized with 6 N hydrochloric acid and buffered with 0.5 M sodium phosphate buffer, pH 7.0−7.2 to generate **2**; Scheme 2.

Reaction of Activated Fluorescein with Maleimide-PNA Labeled Plasmid DNA. The maleimide−PNA labeled plasmid (6.5 nanomol) was immediately reacted with approximately 12-fold excess of fluorescein (**2**) freshly prepared (80 nanomol) in 500 μL 0.5 M sodium phosphate buffer. The reaction mixture was incubated for 30 min at room temperature and the uncoupled **2** was removed by buffer exchange with five washes of 10 mM HEPES buffer (pH 7.4) using 100 kDa Centricon, ultrafiltration centrifugal filter units (YM-100, Millipore, Billerica, MA) and centrifuging at 2000 rpm, for 20 min. The filtrate was discarded and the supernatant consisting of the final conjugate mixture was stored in 10 mM HEPES buffer, pH 7.4, 4 °C, until further use.

Scheme 2. Schematic Illustration of Conjugation of Activated SAMSA Fluorescein to Rhodamine/Maleimide Labeled pGeneGrip-gWIZ Plasmid DNA[a]

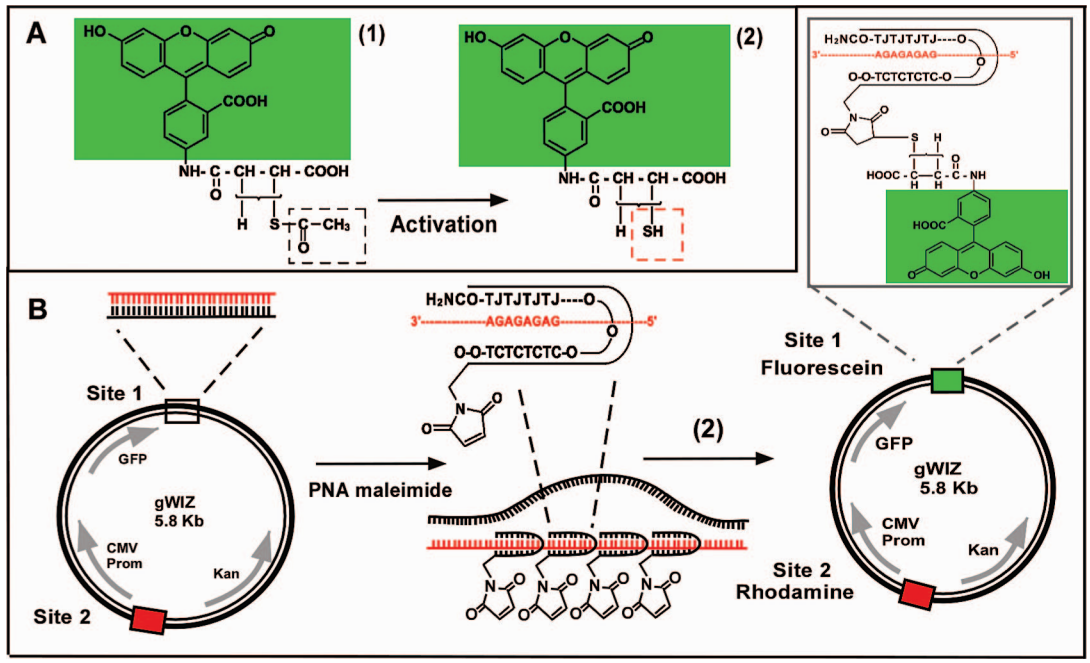

[a] (A) Activation of SAMSA fluorescein (**1**): 0.1 N sodium hydroxide, 15 min incubation; 6 N hydrochloric acid; and 0.5 M sodium phosphate buffer, pH 7.2. This removes the acetyl protecting group in SAMSA fluorescein and exposes the thiol groups (**2**). (B) The free thiol residue on activated SAMSA fluorescein (**2**) covalently reacts with the maleimide group on the plasmid DNA to generate the dual-labeled plasmid DNA.

Agarose Gel Electrophoresis. 0.8% w/v agarose gel electrophoresis was run at 67 V/cm, for 2 h. As a control, a 1 Kb (1 μg/μL) DNA ladder was run by mixing with loading dye (6× solution, 0.25% Bromophenol Blue, 50% glycerol in 1× TAE buffer) (Invitrogen Corp., Carlsbad, CA). Plasmid DNA labeled to rhodamine (Rh) and purified dual-labeled DNA (Rh and activated SAMSA fluorescein) were mixed with a drop of 100% glycerol and 1× TAE buffer prior to electrophoresis. Glycerol was used for sample preparation of the labeled DNA to avoid any interference in fluorophore imaging with the dyes present in the loading dye solution. A Bio-Rad Molecular Imager FX (Hercules, CA) equipped with the appropriate excitation and emission standard filters for Rh and SAMSA fluorescein was used (495/520 nm for fluorescein and 560/590 nm for Rh) to image the labeled DNA bands. The gel was then stained with ethidium bromide nucleic acid stain (final concentration, 0.5 μg/mL) for 30 min followed by three water washes to remove any excess stain and visualized using appropriate filters for ethidium bromide (Ex/Em, 518/605 nm). Bio-Rad Quantity One software was used for analysis of the gel images before and after ethidium bromide staining. The direction of the gel run is shown by (+) and (−) signs.

Restriction Digestion Reaction and Analysis by Gel Electrophoresis. Single and double restriction digestion sites on the dual-labeled pGeneGrip gWIZ-GFP plasmid were identified using New England Biolabs NEBcutter v 2.0 sequence software. The restriction endonucleases *Bam*H1 (20 000 units/mL) and *Pfl*MI (8000 units/mL) (New England BioLabs, Ipswich, MA) were used to digest single and double recognition sites in a non-encoding region of the gWIZ-GFP plasmid, respectively, as shown in the schematic (Scheme 1). The reactants were mixed according to the manufacturers' protocol and incubated for 2 h in a water bath maintained at 37 °C. Gel electrophoresis studies were performed to analyze the digestion reaction fragments (1% w/v agarose, run in 1× TAE buffer, at 67 V/cm, for 1 h). A 1 Kb DNA ladder (1 μg/μL) and purified dual-labeled DNA before digestion were used as controls. *Bam*H1 and *Pfl*MI digested fragments were fully loaded onto the wells in the presence of glycerol prior to gel electrophoresis. Bio-Rad Molecular Imager FX and Quantity One software were used as described above.

Cell Transfection. Transfection studies were conducted in CHO-K1 cells (ATCC, Manassas, VA) by plating 0.5 × 10^6 cells/dish in Bioptechs Delta T dishes (Bioptechs Inc., Butler, PA) one day before the experiment. When the cell population reached 70−80% confluency, they were washed with Hanks' Balanced Salt Solution (HBSS) media, and transfection was carried out in serum-free F12-K media (Invitrogen Corp., Carlsbad, CA). Lipofectamine2000 (Invitrogen Corp., Carlsbad, CA) transfection reagent was used following the manufacturer's protocol. The transfection complexes prepared by complexing dual-labeled DNA conjugates (pGeneGrip gWIZ) (2.76 μg) with Lipofectamine2000 (8.6 μg) at a DNA/lipid ratio of 0.8 μg /2.5 μg w/w were incubated for 15 min before addition to the cells.

Confocal Microscopy. Leica SP2 confocal laser scanning microscope equipped with Ar/Kr, Kr/Ne, and He/Ne lasers (Bannockburn, IL) was used for live cell imaging. Time-lapse imaging with sequential scanning for individual fluorophores was performed following addition of the dual-labeled DNA complexes to CHO-K1 cells. Z-Sectioning was conducted to assist in locating the dual-labeled DNA within the boundaries of the cell membrane. The temperature of the cells during observation was maintained at 37 °C, using a Bioptechs ΔT4 open dish system in a L-15 carbon dioxide free medium.

RESULTS

pGeneGrip gWIZ plasmid DNA containing maleimide/rhodamine groups was successfully dual-labeled via PNA/DNA hybridization using two different PNA linkers at site-1 and site-2 (Scheme 1). The green fluorophore (SAMSA fluorescein) (**1**) was covalently conjugated with the maleimide groups, which are present at site-1, a non-encoding site, as shown in Scheme 2. Prior to the conjugation reaction, (**1**) was activated with sodium hydroxide to remove the acetyl protecting group generating its thiol functionality (**2**). The free thiol moiety on

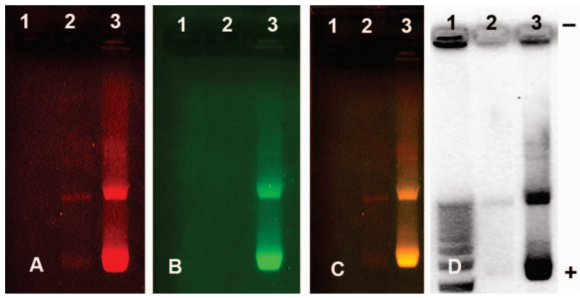

Figure 1. Agarose gel electrophoresis of dual-labeled DNA before and after staining with ethidium bromide DNA stain. Lane 1, DNA ladder; lane 2, DNA labeled with rhodamine (Rh) alone; and lane 3, purified dual-labeled DNA conjugate (Rh (red) and activated SAMSA fluorescein (green)). Panels A and B show exposure at wavelengths that excite the red and the green dyes, respectively. Panel C is the overlap of A and B. Panel D is the UV-excited photoluminescence emission of ethidium bromide (EtBr) stain.

the activated fluorescein was then reacted with the maleimide groups on the plasmid DNA to form a covalent sulfide linkage. pGeneGrip gWIZ plasmid DNA contains approximately 6−10 rhodamine groups and 6−10 PNA−maleimide sites for fluorescein attachment. To maximize conjugation with the plasmid DNA, a 12-fold excess of fluorescein, i.e., a ratio of fluorescein/DNA of 120:1, was used. Unbound fluorophores were removed by ultrafiltration using a 100 kDa membrane (see Materials and Methods section), and this was confirmed by gel electrophoresis. The conjugates remained stable over the 3 month study period.

Gel electrophoresis was used to confirm the dual labeling of plasmid DNA. Detection of the two fluorophores (Rh and fluorescein) conjugated to the DNA was based on direct laser excitation fluorescence imaging using Molecular Imager FX equipped with multichannel excitation and emission filters. The agarose gel revealed two different forms of DNA (lower and higher mobility bands corresponding to open circular forms and supercoiled DNA, respectively) with the majority of the DNA being in the supercoiled conformation (Figure 1). The absence of a band corresponding to rhodamine-labeled DNA upon excitation for fluorescein confirmed lack of any spectral overlap between the two fluorophores used (Figure 1A,B, lane 2). The overlap of panels A and B resulted in yellow bands in lane 3 due to the close proximity of the fluorophores (red and green) on the intact dual-labeled DNA (Figure 1C, lane 3). For comparison, ethidium bromide stained DNA bands are shown in Figure 1D.

To simulate DNA degradation, a model experiment was conducted using the restriction endonucleases *Bam*H1 and *Pfl*MI that cut the plasmid DNA in non-encoding regions at specific single and double recognition sites, respectively (Scheme 1). Gel electrophoresis confirmed the different DNA digestion fragments (Figure 2). Panels A and B in Figure 2 show the emission bands of rhodamine and fluorescein, respectively, after separate excitation using the appropriate filters. Prior to the addition of the restriction enzymes, the DNA bands (open circular and supercoiled forms) are yellow due to the close proximity of the red and green labels on the intact DNA (Figure 2C, lane 2). Upon digestion with the restriction enzyme (*Bam*H1) that cuts at a single site, the circular DNA is linearized, resulting in a single linear strand which has a lower mobility than the supercoiled DNA in lane 2. This linearized DNA is visualized as a yellow band due to the close proximity of the fluorophores (Figure 2C, lane 3). Upon addition of the restriction enzyme *Pfl*MI, which cuts the DNA into two fragments (dual site cutter), the DNA is seen as individual red and green bands, as the two fluorophores are now separated (Figure 2C, lane 4). The DNA fragment containing rhodamine has a lower molecular weight than the fragment containing fluorescein. This difference is observed on the gel electrophoresis with the rhodamine-containing DNA fragment possessing higher mobility than the fluorescein-containing fragment.

On the basis of these observations, dual-labeled DNA was used to explore intracellular trafficking of DNA following transfection in CHO-K1 cells with the cationic liposome, Lipofectamine2000. The lipoplexes containing DNA conjugates were observed using confocal imaging at both the red and green channels (Figure 3I). At the initial time point prior to cellular uptake, imaging was conducted at a focal plane above the cells (0 h, Figure 3I). The overlapped image is visualized as yellow fluorescent voxels due to colocalization of the red and green fluorophores on the intact DNA. Live cell time-lapse imaging at various time points over a 3 h period showed the uptake and intracellular distribution of the DNA conjugates (Figure 3). Optical Z-sectioning was performed to locate the labeled DNA within the boundaries of the cell. Time-lapse imaging at 1, 2, and 3 h revealed yellow as well as individual red and green fluorescent voxels (Figure 3II, A−C) shown by arrows and enlarged images (B1 and C1). The uptake of the DNA conjugates increased with time with only a few conjugates observed at 1 h. At the 1 h time point (Figure 3IIA), only 18% of cells showed uptake of labeled DNA. By 2 h (Figure 3IIB), ∼59% of cells showed uptake of labeled DNA, with ∼32% of cells showing color separation due to DNA degradation. At the 3 h time point (Figure 3IIC), ∼72% of the cells showed uptake of the labeled DNA, with 41% of cells showing DNA degradation.

DISCUSSION

The methodology reported here to dual-label plasmid DNA through PNA linkers shows promise as a bioimaging tool to efficiently elucidate intracellular DNA degradation. pGeneGrip plasmid DNA contains rhodamine fluorophores. SAMSA fluorescein (green) was chosen as a second fluorophore due to its efficient coupling to the pendant maleimide groups on the plasmid DNA. This dual-labeling method did not change the mobility or the supercoiled conformation of the plasmid DNA as confirmed by gel electrophoresis studies.

Gel electrophoresis studies following restriction enzyme digestion demonstrated the utility of dual-labeled plasmid DNA to visualize differences in the plasmid DNA when intact or degraded. This study confirmed visualization of the undigested intact plasmid DNA as a yellow color (due to the close proximity of the two fluorophore labels) with the majority being in the supercoiled form. On the other hand, fragmented DNA, cut at the *Pfl*MI sites (Scheme 1), was seen as two colors (red and green), due to separation of the two fluorophores. The DNA that had undergone only a single site cut (i.e., linearized plasmid DNA) at the *Bam*H1 site is visualized as a yellow color. This could lead to discrepancies in the discrimination of intracellular DNA degradation fragments during tracking studies, since degradation must be at an advanced stage (i.e., beyond at least a single cut) before it can be detected using this methodology. There is a good probability of two or more double strand breaks to occur in a single plasmid intracellularly, since at the onset of endonuclease activity, exonucleases will quickly start the degradation process at the free ends of linearized DNA. Although the possibility of a single cut in DNA is unlikely, a normalization factor can be developed to account for the nondiscernable single cut event. This normalization factor can be determined as a function of enzymatic digestion measured using gel electrophoresis. Single cut and intact DNA can be distinguished in gel electrophoresis, since the single cut DNA, which cannot be in the supercoiled form, has a different mobility (lane 3, Figure 2).

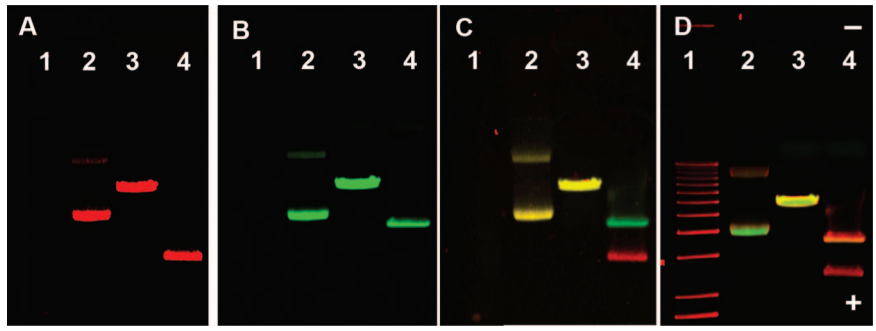

Figure 2. Agarose gel electrophoresis of dual-labeled DNA after treatment with *Bam*H1 and *Pfl*MI restriction enzymes. Lane 1, DNA ladder; lane 2, dual-labeled DNA (Rh (red) and activated SAMSA fluorescein (green)) before digestion; lane 3, *Bam*H1 treated (single site cutter); lane 4, *Pfl*MI treated (two site cutter). Panels A and B show exposure at wavelengths that excite the red and the green dyes, respectively. Panel C is the overlap of A and B. Panel D is the overlapped image after ethidium bromide (EtBr) staining. In panel C, the yellow bands in lanes 2 (DNA before digestion) and 3 (linearized DNA after *Bam*H1 digestion) are due to the close proximity of the red and green dyes on the DNA, whereas in lane 4, the red and green colors are separated after *Pfl*MI digestion at two sites. In panel D, EtBr staining compromises the dye colors in lanes 2−4.

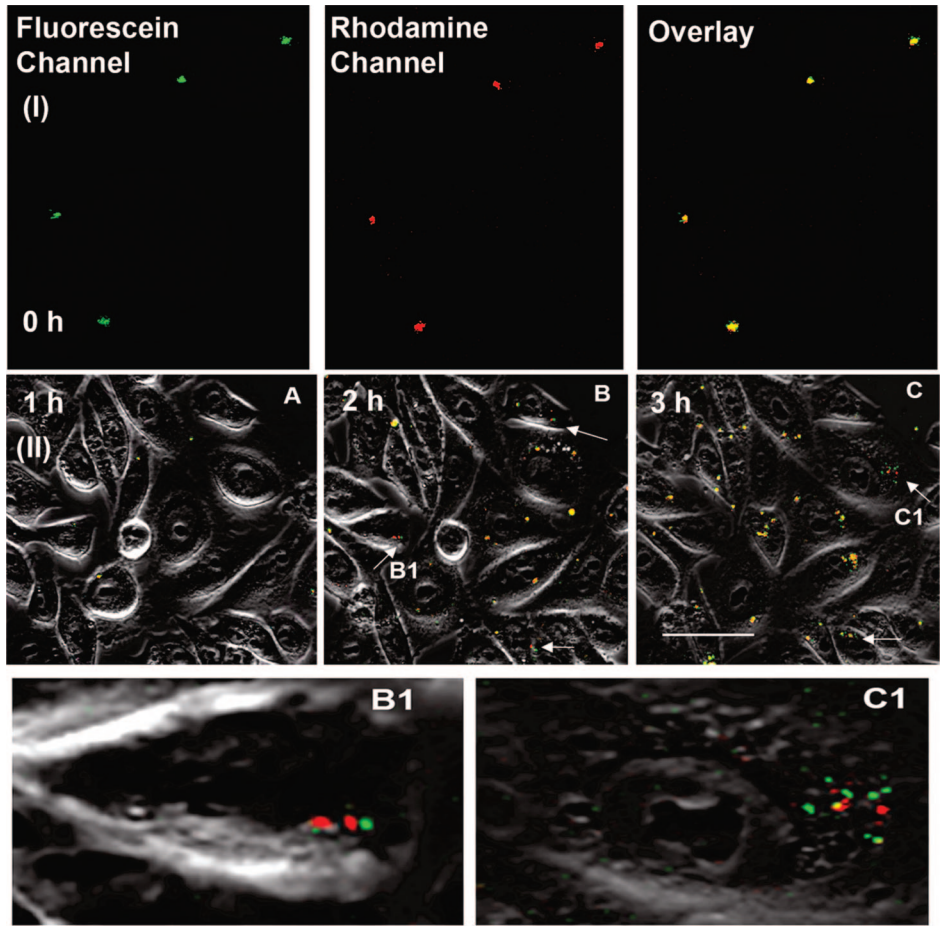

Figure 3. Confocal imaging for uptake of dual-labeled plasmid DNA (rhodamine and activated SAMSA fluorescein) incubated for 0−3 h in the presence of Lipofectamine2000 in CHO-K1 cells. (I) Sequential scanning at the initial time point (0 h). Panels are shown in the following order: green fluorescence (activated SAMSA fluorescein); red fluorescence (rhodamine); and overlap of red and green channels. (II) Time-lapse imaging with sequential scanning for 0−3 h post-transfection (bar 10 μm). Panels A−C overlapped images of all channels at 1, 2, and 3 h, respectively, and revealed yellow as well as individual red and green fluorescent voxels shown by arrows and enlarged images (B1 and C1). The yellow fluorescent voxels in the overlapped images are due to the close proximity of green and red fluorophores in intact dual-labeled DNA. The uptake of the DNA conjugates increased with time with only a few conjugates observed at 1 h. The amount of red and green separation also appears to increase with time (as shown in B1 and C1), indicating progressive DNA degradation.

The practical application of dual-labeled DNA to indicate DNA instability was verified following uptake in CHO-K1 cells using confocal microscopy. The combination of time-lapse imaging and dual-labeled DNA tracking revealed yellow fluorescent voxels in the cytosplasm (which likely represent intact plasmids), as well as color separation, which is indicative of DNA degradation. The yellow fluorescent voxels, evident in the cytoplasm at the 1, 2, and 3 h time points post-transfection, indicate that this DNA is probably in the supercoiled form and/or protected by the cationic liposome vector. Lechardeur et al. reported that lipid-encapsulated plasmid DNA enhanced the stability to degradation (∼25%) when compared to naked plasmid DNA (∼75%) within 4 h after microinjection into the cytosol (*31*). Supercoiled DNA is less susceptible to degradation by cytosolic nucleases, especially endoexonucleases when compared to linearized plasmid or open, circular forms of

plasmid DNA (*42*−*45*). In addition, the more compact nature of supercoiled DNA increases diffusion through the actin and mictrotubular network, thereby allowing a more rapid migration toward the perinuclear region when compared to linear DNA (*42*).

At the 1 h time point post-transfection, only a few yellow fluorescent voxels were seen and there was no red and green separation. The low number of yellow fluorescent voxels observed at the 1 h time point is due to incomplete uptake. This is in agreement with our previous studies, which revealed that maximum uptake of these complexes occurred at approximately 3 h in CHO-K 1 cells (*19*). The amount of red and green separation also appears to increase with time (as shown in Figure 3II), indicating progressive DNA degradation.

Since cationic lipoplexes are generally taken up via the endosomal route (*46*), it is possible that the degradation observed may be due to either entrapment of some complexes in the lysosomal compartment (*33, 46*) or degradation by cytosolic nucleases following release from the endosomes (*31, 46*−*48*). To further elucidate this, future experiments will require labeling of the various subcellular compartments. To address any complexity involved in detection of colocalization or fluorophore separation, we propose to label DNA using similar technology at more than two sites. Imaging of DNA conjugates longer than 3 h was not feasible due to photobleaching of the conjugated fluorophores. This is expected to be alleviated by the use of quantum dots as opposed to organic fluorophores (*19*). Nevertheless, this technique enabled observation of DNA degradation within cells by concurrent tracking using confocal time-lapse imaging. It is anticipated that the use of the dual-labeling technique described here, in combination with organelle stains and nuclease inhibitors (*30, 31, 34, 45, 49*), will be very valuable in elucidating inefficiencies at the different DNA cellular trafficking stages.

CONCLUSIONS

Plasmid DNA was successfully dual-labeled with rhodamine and fluorescein at two separate sites. Gel electrophoresis confirmed the mobility and structural integrity of the dual-labeled DNA. Cellular DNA degradation, simulated using restriction endonucleases, revealed intact DNA as a single color and degraded DNA as two separate colors. Confocal time-lapse imaging and intracellular tracking studies enabled simultaneous visualization of DNA distribution and degradation. A major limitation of this study was the photo-instability of the organic fluorophores used, which significantly limited the time over which DNA tracking at a single cell level could be conducted. More stable fluorophores, such as quantum dots (*19, 50*−*52*) as described in our previous work (*19*), could be used to perform long-term tracking studies.

ACKNOWLEDGMENT

We thank the UCONN Flow Cytometry/Confocal Microscopy core facility for use of instrumentation. This research was supported in part by the Parenteral Drug Association Foundation Schering-Plough Grant, NSF DMI 0303950, ONR N000LY0610016PR, and ARO DAAD-02-1-0381.

LITERATURE CITED

(1) Wolff, J. A., and Rozema, D. B. (2008) Breaking the bonds: non-viral vectors become chemically dynamic. *Mol. Ther. 16*, 8–15.
(2) Wasungu, L., and Hoekstra, D. (2006) Cationic lipids, lipoplexes and intracellular delivery of genes. *J. Controlled Release 116*, 255–64.
(3) Nabel, G. J. (2004) Genetic, cellular and immune approaches to disease therapy: past and future. *Nat. Med. 10*, 135–41.
(4) Luo, D., and Saltzman, W. M. (2000) Synthetic DNA delivery systems. *Nat. Biotechnol. 18*, 33–37.
(5) Patil, S. D., Rhodes, D. G., and Burgess, D. J. (2005) DNA-based therapeutics and DNA delivery systems: a comprehensive review. *AAPS J. 7*, E61−77.
(6) Rolland, A. (2005) Gene medicines: The end of the beginning? *Adv. Drug Delivery Rev. 57*, 669–673.
(7) Pouton, C. W., and Seymour, L. W. (1998) Key issues in non-viral gene delivery. *Adv. Drug Delivery Rev. 34*, 3–19.
(8) Wiethoff, C. M., and Middaugh, C. R. (2003) Barriers to nonviral gene delivery. *J. Pharm. Sci. 92*, 203–17.
(9) Joshee, N., Bastola, D. R., and Cheng, P. W. (2002) Transferrin-facilitated lipofection gene delivery strategy: characterization of the transfection complexes and intracellular trafficking. *Hum. Gene Ther. 13*, 1991–2004.
(10) Simoes, S., Slepushkin, V., Pires, P., Gaspar, R., de Lima, M. P., and Duzgunes, N. (1999) Mechanisms of gene transfer mediated by lipoplexes associated with targeting ligands or pH-sensitive peptides. *Gene Ther. 6*, 1798–807.
(11) Khalil, I. A., Kogure, K., Akita, H., and Harashima, H. (2006) Uptake pathways and subsequent intracellular trafficking in nonviral gene delivery. *Pharmacol. Rev. 58*, 32–45.
(12) El Ouahabi, A., and Ruysschaert, J.-M. (2005) Formation and intracellular trafficking of lipoplexes and polyplexes. *Mol. Ther. 11*, 336–347.
(13) Favaro, E., and Indraccolo, S. (2007) Gene therapy of cancer in the clinic: good news in sight from Asia? *Curr. Opin. Mol. Ther. 9,* 477−82.
(14) Rejman, J., Conese, M., and Hoekstra, D. (2006) Gene transfer by means of lipo- and polyplexes: role of clathrin and caveolae-mediated endocytosis. *J. Liposome Res. 16*, 237–47.
(15) Manunta, M., Nichols, B. J., Tan, P. H., Sagoo, P., Harper, J., and George, A. J. (2006) Gene delivery by dendrimers operates via different pathways in different cells, but is enhanced by the presence of caveolin. *J. Immunol. Meth. 314*, 134–46.
(16) Radler, J. O., Koltover, I., Salditt, T., and Safinya, C. R. (1997) Structure of DNA-cationic liposome complexes: DNA intercalation in multilamellar membranes in distinct interhelical packing regimes. *Science 275*, 810–4.
(17) Chesnoy, S., and Huang, L. (2000) Structure and function of lipid-DNA complexes for gene delivery. *Annu. Rev. Biophys. Biomol. Struct. 29*, 27–47.
(18) Goncalves, C., Mennesson, E., Fuchs, R., Gorvel, J. P., Midoux, P., and Pichon, C. (2004) Macropinocytosis of polyplexes and recycling of plasmid via the clathrin-dependent pathway impair the transfection efficiency of human hepatocarcinoma cells. *Mol. Ther. 10*, 373–85.
(19) Srinivasan, C., Lee, J., Papadimitrakopoulos, F., Silbart, L. K., Zhao, M., and Burgess, D. J. (2006) Labeling and intracellular tracking of functionally active plasmid DNA with semiconductor quantum dots. *Mol. Ther. 14*, 192–201.
(20) Panyam, J., and Labhasetwar, V. (2003) Biodegradable nanoparticles for drug and gene delivery to cells and tissue. *Adv. Drug Delivery Rev. 55*, 329–47.
(21) Bally, M. B., Harvie, P., Wong, F. M., Kong, S., Wasan, E. K., and Reimer, D. L. (1999) Biological barriers to cellular delivery of lipid-based DNA carriers. *Adv. Drug Delivery Rev. 38*, 291–315.
(22) Lechardeur, D., Verkman, A. S., and Lukacs, G. L. (2005) Intracellular routing of plasmid DNA during non-viral gene transfer. *Adv. Drug Delivery Rev. 57*, 755–767.
(23) Simoes, S., Slepushkin, V., Gaspar, R., Lima, M. C. d., and Duzgunes, N. (1998) Gene delivery by negatively charged ternary complexes of DNA, cationic liposomes and transferrin or fusigenic peptides. *Gene Ther. 5*, 955–64.
(24) Hope, M. J., Mui, B., Ansell, S., and Ahkong, Q. F. (1998) Cationic lipids, phosphatidylethanolamine and the intracellular delivery of polymeric, nucleic acid-based drugs. *Mol. Membr. Biol. 15*, 1–14.
(25) Godbey, W. T., Wu, K. K., and Mikos, A. G. (1999) Poly(ethylenimine) and its role in gene delivery. *J. Controlled*

Release 60, 149–160.
(26) Fraser, M. J., Tynan, S. J., Papaioannou, A., Ireland, C. M., and Pittman, S. M. (1996) Endo-exonuclease of human leukaemic cells: evidence for a role in apoptosis. *J. Cell Sci. 109*, 2343–60 (Pt 9).
(27) Lacks, S. A. (1981) Deoxyribonuclease I in mammalian tissues. Specificity of inhibition by actin. *J. Biol. Chem. 256*, 2644–8.
(28) Escriou, V., Carriere, M., Scherman, D., and Wils, P. (2003) NLS bioconjugates for targeting therapeutic genes to the nucleus. *Adv. Drug Delivery Rev. 55*, 295–306.
(29) Neves, C., Escriou, V., Byk, G., Scherman, D., and Wils, P. (1999) Intracellular fate and nuclear targeting of plasmid DNA. *Cell Biol. Toxicol. 15*, 193–202.
(30) Pollard, H., Toumaniantz, G., Amos, J. L., Avet-Loiseau, H., Guihard, G., Behr, J. P., and Escande, D. (2001) Ca^{2+}-sensitive cytosolic nucleases prevent efficient delivery to the nucleus of injected plasmids. *J. Gene Med. 3*, 153–64.
(31) Lechardeur, D., Sohn, K. J., Haardt, M., Joshi, P. B., Monck, M., Graham, R. W., Beatty, B., Squire, J., O'Brodovich, H., and Lukacs, G. L. (1999) Metabolic instability of plasmid DNA in the cytosol: a potential barrier to gene transfer. *Gene Ther. 6*, 482–97.
(32) Briane, D., Lesage, D., Cao, A., Coudert, R., Lievre, N., Salzmann, J. L., and Taillandier, E. (2002) Cellular pathway of plasmids vectorized by cholesterol-based cationic liposomes. *J. Histochem. Cytochem. 50*, 983–91.
(33) Zabner, J., Fasbender, A. J., Moninger, T., Poellinger, K. A., and Welsh, M. J. (1995) Cellular and molecular barriers to gene transfer by a cationic lipid. *J. Biol. Chem. 270*, 18997–9007.
(34) Cornelis, S., Vandenbranden, M., Ruysschaert, J. M., and Elouahabi, A. (2002) Role of intracellular cationic liposome-DNA complex dissociation in transfection mediated by cationic lipids. *DNA Cell Biol. 21*, 91–7.
(35) Jones, R. A., Cheung, C. Y., Black, F. E., Zia, J. K., Stayton, P. S., Hoffman, A. S., and Wilson, M. R. (2003) Poly(2-alkylacrylic acid) polymers deliver molecules to the cytosol by pH-sensitive disruption of endosomal vesicles. *Biochem. J. 372*, 65–75.
(36) Fernandez, B., Galvez, N., Sanchez, P., Cuesta, R., Bermejo, R., and Dominguez-Vera, J. M. (2007) Fluorescence resonance energy transfer in ferritin labeled with multiple fluorescent dyes. *J. Biol. Inorg. Chem.*
(37) Zelphati, O., and Szoka, F. C., Jr. (1996) Intracellular distribution and mechanism of delivery of oligonucleotides mediated by cationic lipids. *Pharm. Res. 13*, 1367–72.
(38) Noguchi, A., Furuno, T., Kawaura, C., and Nakanishi, M. (1998) Membrane fusion plays an important role in gene transfection mediated by cationic liposomes. *FEBS Lett. 433*, 169–73.
(39) Zelphati, O., Liang, X., Hobart, P., and Felgner, P. L. (1999) Gene chemistry: functionally and conformationally intact fluorescent plasmid DNA. *Hum. Gene Ther. 10*, 15–24.
(40) Zelphati, O., Liang, X., Nguyen, C., Barlow, S., Sheng, S., Shao, Z., and Felgner, P. L. (2000) PNA-dependent gene chemistry: stable coupling of peptides and oligonucleotides to plasmid DNA. *Biotechniques. 28*, 304–10, 312−4, 316.
(41) Tanimoto, M., Kamiya, H., Minakawa, N., Matsuda, A., and Harashima, H. (2003) No enhancement of nuclear entry by direct conjugation of a nuclear localization signal peptide to linearized DNA. *Bioconjugate Chem. 14*, 1197–202.
(42) Remaut, K., Sanders, N. N., Fayazpour, F., Demeester, J., and De Smedt, S. C. (2006) Influence of plasmid DNA topology on the transfection properties of DOTAP/DOPE lipoplexes. *J. Controlled Release 115*, 335–43.
(43) Cherng, J. Y., Schuurmans-Nieuwenbroek, N. M., Jiskoot, W., Talsma, H., Zuidam, N. J., Hennink, W. E., and Crommelin, D. J. (1999) Effect of DNA topology on the transfection efficiency of poly((2-dimethylamino)ethyl methacrylate)-plasmid complexes. *J. Controlled Release 60*, 343–53.
(44) Glasspool-Malone, J., and Malone, R. W. (1999) Marked enhancement of direct respiratory tissue transfection by aurintricarboxylic acid. *Hum. Gene Ther. 10*, 1703–13.
(45) Ross, G. F., Bruno, M. D., Uyeda, M., Suzuki, K., Nagao, K., Whitsett, J. A., and Korfhagen, T. R. (1998) Enhanced reporter gene expression in cells transfected in the presence of DMI-2, an acid nuclease inhibitor. *Gene Ther. 5*, 1244–50.
(46) Xu, Y., and Szoka, F. C., Jr. (1996) Mechanism of DNA release from cationic liposome/DNA complexes used in cell transfection. *Biochemistry 35*, 5616–23.
(47) Zabner, J. (1997) Cationic lipids used in gene transfer. *Adv. Drug Delivery Rev. 27*, 17–28.
(48) Zuhorn, I. S., Kalicharan, R., and Hoekstra, D. (2002) Lipoplex-mediated transfection of mammalian cells occurs through the cholesterol-dependent clathrin-mediated pathway of endocytosis. *J. Biol. Chem. 277*, 18021–8.
(49) Torriglia, A., Chaudun, E., Courtois, Y., and Counis, M. F. (1997) On the use of Zn2+ to discriminate endonucleases activated during apoptosis. *Biochimie 79*, 435–8.
(50) Gao, X., Yang, L., Petros, J. A., Marshall, F. F., Simons, J. W., and Nie, S. (2005) In vivo molecular and cellular imaging with quantum dots. *Curr. Opin. Biotechnol. 16*, 63–72.
(51) Watson, A., Wu, X., and Bruchez, M. (2003) Lighting up cells with quantum dots. *Biotechniques 34*, 296–300, 302−3.
(52) Alivisatos, A. P., Gu, W., and Larabell, C. (2005) Quantum dots as cellular probes. *Annu. Rev. Biomed. Eng. 7*, 55–76.

BC800184J